




## Orai, RyR, and IP<sub>3</sub>R channels cooperatively regulate calcium signaling in brain mid-capillary pericytes

Braxton Phillips<sup>1,2,3</sup> , Jenna Clark<sup>1,2,3</sup>, Éric Martineau<sup>2,3</sup>  & Ravi L. Rungta<sup>2,3</sup> ✉

Pericytes are multifunctional cells of the vasculature that are vital to brain homeostasis, yet many of their fundamental physiological properties, such as Ca<sup>2+</sup> signaling pathways, remain unexplored. We performed pharmacological and ion substitution experiments to investigate the mechanisms underlying pericyte Ca<sup>2+</sup> signaling in acute cortical brain slices of PDGFRβ-Cre::GCaMP6f mice. We report that mid-capillary pericyte Ca<sup>2+</sup> signalling differs from ensheathing type pericytes in that it is largely independent of L- and T-type voltage-gated calcium channels. Instead, Ca<sup>2+</sup> signals in mid-capillary pericytes were inhibited by multiple Orai channel blockers, which also inhibited Ca<sup>2+</sup> entry triggered by endoplasmic reticulum (ER) store depletion. An investigation into store release pathways indicated that Ca<sup>2+</sup> transients in mid-capillary pericytes occur through a combination of IP<sub>3</sub>R and RyR activation, and that Orai store-operated calcium entry (SOCE) is required to sustain and amplify intracellular Ca<sup>2+</sup> increases evoked by the GqGPCR agonist endothelin-1. These results suggest that Ca<sup>2+</sup> influx via Orai channels reciprocally regulates IP<sub>3</sub>R and RyR release pathways in the ER, which together generate spontaneous Ca<sup>2+</sup> transients and amplify Gq-coupled Ca<sup>2+</sup> elevations in mid-capillary pericytes. Thus, SOCE is a major regulator of pericyte Ca<sup>2+</sup> and a target for manipulating their function in health and disease.

<sup>1</sup>Department of Neuroscience, Université de Montréal, Montréal, QC, Canada. <sup>2</sup>Department of Stomatology, Faculty of Dental Medicine, Université de Montréal, Montréal, QC H3C3J7, Canada. <sup>3</sup>Centre interdisciplinaire de recherche sur le cerveau et l'apprentissage, Université de Montréal, Montréal, QC, Canada. ✉email: [ravi.rungta@umontreal.ca](mailto:ravi.rungta@umontreal.ca)

The mural cells of the brain are multifunctional cells organized in a continuum along the arterio-venous axis of the cerebral vasculature. This continuum is grouped into distinct cell types, which includes smooth muscle cells on penetrating arterioles (aSMCs), pre-capillary sphincters and ensheathing pericytes (also named terminal SMCs) of the arteriole-to-capillary transition zone, pericytes of the mid-capillary bed (of mesh and thin-strand morphology – here collectively referred to as mid-capillary pericytes), and venule smooth muscle cells<sup>1,2</sup>. Although they share a common origin<sup>3</sup> and similar nomenclature, these cell types have numerous morphological<sup>4,5</sup>, transcriptomic<sup>6,7</sup>, and functional differences<sup>8,9</sup>. For example, aSMCs and ensheathing pericytes fully encircle and exhibit near complete coverage of the endothelial tube, highly express alpha smooth muscle actin ( $\alpha$ -SMA), and undoubtedly regulate cerebral blood flow (CBF)<sup>9,10</sup>. Mid-capillary pericytes have thin or mesh-like processes that run longitudinal to the vessel, express little to no  $\alpha$ -SMA, and their role in controlling CBF in physiological contexts remains poorly defined. Nevertheless, blood flow control aside, mid-capillary pericytes have numerous functions in health and disease, such as blood–brain-barrier regulation<sup>11–13</sup> neuroimmune regulation<sup>14</sup>, angiogenesis<sup>15</sup>, glial scar formation<sup>16</sup>, and suggested stem cell-like properties<sup>17</sup>. Yet, despite these important functions, the basic physiological properties of brain mid-capillary pericytes, including the mechanisms that regulate their  $\text{Ca}^{2+}$  signaling, remain understudied.

All mural cells exhibit spontaneous fluctuations in intracellular  $\text{Ca}^{2+}$ , which are termed  $\text{Ca}^{2+}$  transients<sup>9,18,19</sup>. Whereas the mechanisms underlying calcium signaling and contraction in aSMCs have been studied in detail (e.g. refs. <sup>20–26</sup>), investigations into brain pericyte  $\text{Ca}^{2+}$  signaling mechanism are only beginning to emerge. In ensheathing-type pericytes,  $\text{Ca}^{2+}$  transients can be caused by transmembrane influx through voltage-gated  $\text{Ca}^{2+}$  channels (VGCCs) and inositol 1,4,5-trisphosphate receptor (IP3R) signaling that recruits the  $\text{Ca}^{2+}$  required for  $\alpha$ -SMA-mediated contraction<sup>27,28</sup>. Mid-capillary pericytes also exhibit  $\text{Ca}^{2+}$  transients with similar properties in vivo and in vitro, which are confined to spatial microdomains and modulated by neuronal activity<sup>9,18,29</sup>. Interestingly, a recent study reported that in resting conditions mid-capillary pericyte  $\text{Ca}^{2+}$  transients were only minimally sensitive to the potent L-type VGCC blocker nimodipine but were largely inhibited by the non-selective ion channel blocker SKF-96365<sup>18</sup>, consistent with a prior study reporting reduced functional expression of VGCCs on distal retinal capillaries<sup>30</sup>. In addition to non-selective cation TRPC channels, SKF-96365 blocks several other  $\text{Ca}^{2+}$  channels that are highly expressed in mid-capillary pericytes such as T-type VGCCs<sup>31</sup>, and the Orai family of store-operated  $\text{Ca}^{2+}$  channels<sup>32</sup>. Mid-capillary pericytes also express a plethora of Gq-coupled receptors<sup>7,33</sup>, which when activated would be expected to trigger  $\text{Ca}^{2+}$  release from internal stores via IP3R signaling. Therefore, a more detailed investigation is required to understand the cellular mechanisms underlying  $\text{Ca}^{2+}$  signaling in mid-capillary pericytes, their voltage dependence, and the interplay between  $\text{Ca}^{2+}$  release from internal stores and transmembrane influx.

Here, we utilized pharmacology experiments on acute cortical brain slices from transgenic mice expressing a fluorescent calcium indicator, GCaMP6f, in brain mural cells expressing PDGFR $\beta$  (PDGFR $\beta$ -Cre;GCaMP6f mice) to delineate the mechanisms underlying  $\text{Ca}^{2+}$  signaling in brain pericytes. Surprisingly, in contrast to ensheathing type pericytes which we show exhibit  $\text{Ca}^{2+}$  transients that are partially dependent on VGCCs, mid-capillary pericyte  $\text{Ca}^{2+}$  signals are largely unaffected by inhibition of VGCCs. We show that mid-capillary pericyte  $\text{Ca}^{2+}$  transients are, instead, primarily mediated by an interplay between store-operated  $\text{Ca}^{2+}$  entry (SOCE) channels and release of  $\text{Ca}^{2+}$  from

internal stores by IP3Rs and ryanodine receptors (RyRs). Underscoring the potential importance of pericyte SOCE channels, we further demonstrate that they amplify Gq-coupled  $[\text{Ca}^{2+}]_i$  elevations evoked by the potent vasoconstrictor endothelin-1 (ET-1).

## Results

Pericyte  $\text{Ca}^{2+}$  signals were visualized with confocal imaging in acute cortical slices from PDGFR $\beta$ -Cre;GCaMP6f mice. The capillary lumen was labeled with an intravenous (I.V.) injection of RhodamineB-Dextran (70 kDa) and pericyte somas were labeled with the recently described pericyte specific dye TO-PRO-3<sup>34</sup> (Fig. 1a). The spontaneous and spatially incoherent nature of mid-capillary pericyte  $\text{Ca}^{2+}$  transients led us to take advantage of the recently developed event-based analysis tool AQuA, which was developed precisely for unbiased analysis of such signals, but in astrocytes<sup>35</sup>. When applied to pericytes, AQuA was found suitable for extracting several properties of these pericyte  $\text{Ca}^{2+}$  transients, such as overall event frequency, amplitude, area, and duration (Fig. S1a–c; Supplementary Movie 1; and Tables S1 and S2). Indeed,  $\text{Ca}^{2+}$  transient frequency in mid-capillary pericyte somas as measured by AQuA was well-matched to measurements made with a region-of-interest based approach (Fig. 1b–d and S1d).

We first tested whether these  $\text{Ca}^{2+}$  transients depended on extracellular  $\text{Ca}^{2+}$  ( $[\text{Ca}^{2+}]_{ex}$ ) by washing out  $[\text{Ca}^{2+}]_{ex}$  from the perfused artificial cerebral spinal fluid (ACSF). Perfusion of 0 mM  $\text{Ca}^{2+}$ , 2 mM EGTA solution reversibly depressed the frequency of  $\text{Ca}^{2+}$  transients in both the processes and soma of the pericyte (Fig. 1b–e and S1b–d). The inhibition of  $\text{Ca}^{2+}$  transients by  $\text{Ca}^{2+}$ -free solution was rapid, reaching a maximal effect within 5–9 min (Fig. S1e). To test whether intracellular  $\text{Ca}^{2+}$  stores were completely depleted following 10 min in  $\text{Ca}^{2+}$ -free ACSF, we applied Gq-coupled GPCR agonists for either the endothelin (ET)-A or thromboxane A2 receptor, ET-1 and U46619 respectively, which increase intracellular pericyte  $\text{Ca}^{2+}$  in an IP3-dependent manner. ET-1 and U46619 were still able to evoke  $\text{Ca}^{2+}$  transients in  $\text{Ca}^{2+}$ -free solution (Fig. 1f, g), suggesting that  $\text{Ca}^{2+}$  stores were not fully depleted at this time point. However, after prolonged exposure to  $\text{Ca}^{2+}$  free solution (30 min) signals generated by ET-1 application were severely blunted when compared to those induced at 5 and 10 min following  $[\text{Ca}^{2+}]_{ex}$  removal (Fig. S2), suggesting a gradual run down of store  $\text{Ca}^{2+}$  levels in the absence of transmembrane  $\text{Ca}^{2+}$  influx, and a dependence on  $[\text{Ca}^{2+}]_{ex}$  to maintain ER store  $\text{Ca}^{2+}$ . Intriguingly, in  $\text{Ca}^{2+}$  free solution the ET-1 and U46619 induced increases in  $\text{Ca}^{2+}$  transient frequency were temporary (ET-1,  $248.2 \pm 46.52$  s; U46619,  $268.6 \pm 32.65$  s) (Fig. S2a) in contrast to the sustained global elevation previously observed in normal  $[\text{Ca}^{2+}]_{ex}$  solution<sup>18</sup>. Altogether, these results suggest mid-capillary pericyte  $\text{Ca}^{2+}$  transients require a plasmalemmal influx pathway, either to directly generate the transients or to sustain constitutive intracellular store filling and release.

In ensheathing pericytes, depolarization triggers transmembrane influx of  $\text{Ca}^{2+}$  via VGCCs, thereby increasing  $\text{Ca}^{2+}$  transient frequency and  $[\text{Ca}^{2+}]_i$ <sup>27,28</sup>. Therefore, we tested the effect of blocking the predominantly expressed pericyte VGCC subtypes,  $\text{Ca}_v1.2$  (L-type) and  $\text{Ca}_v3.2$  (T-type), with nifedipine and Z944<sup>36</sup>, respectively (Fig. 2a). Application of nifedipine (20  $\mu\text{M}$ ) and Z944 (2  $\mu\text{M}$ ) had no effect on the frequency of  $\text{Ca}^{2+}$  transients, or baseline  $\text{Ca}^{2+}$  levels, in either the processes or soma (Fig. 2b, S4, and Tables S1 and S2). However, we could not exclude the possibility that VGCC transients would become more apparent if the membrane were depolarized, as previously reported for ensheathing type pericytes<sup>27</sup>. Consistent with this previous report,  $\text{Ca}^{2+}$  transient frequency of ensheathing

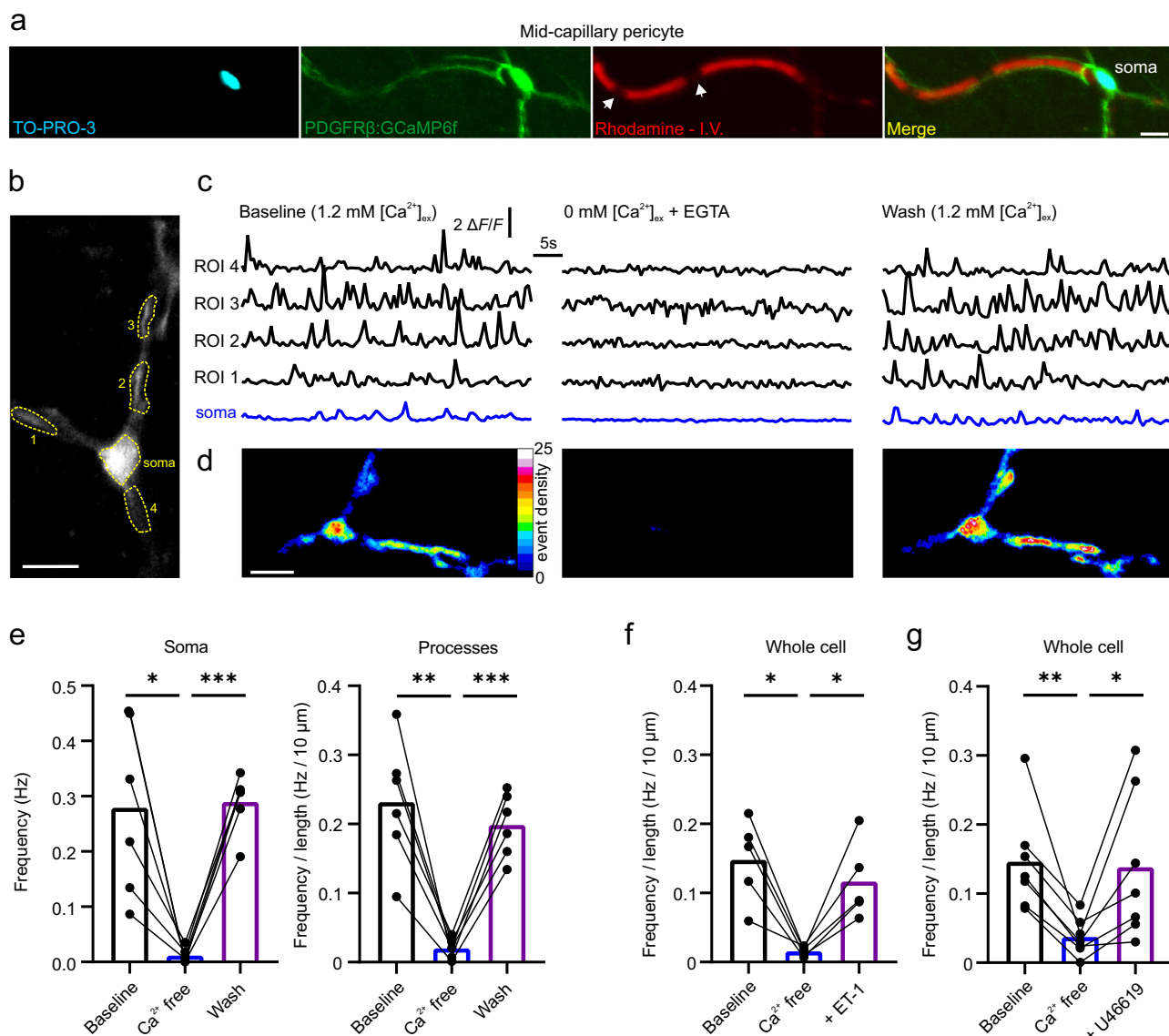


**Fig. 1** Imaging of mid-capillary pericyte  $\text{Ca}^{2+}$  transients and their dependence on extracellular  $\text{Ca}^{2+}$ . **a** Confocal z-projection of a pericyte expressing GCaMP6f (green) in an acute brain slice loaded with TO-PRO-3 (cyan) and contacting a capillary whose lumen is labeled with RhodamineB-dextran (Red) – arrow heads indicate red blood cells. **b** Image of a GCaMP6f fluorescent pericyte and ROIs selected for **c**. **c** ROI based analysis of fluorescence changes in ROIs from (**b**) at baseline (left), after 11 min in  $\text{Ca}^{2+}$  free ACSF (middle), and 5 min following wash back of  $\text{Ca}^{2+}$  containing ACSF (right). **d** Heat maps of pericyte from (**b**, **c**) showing event density calculated from AQUA (percent time each pixel is active) in same conditions as above in **c**. **e** Summarized data showing effect of transiently removing and washing back  $[\text{Ca}^{2+}]_{\text{ex}}$  on pericyte  $\text{Ca}^{2+}$  transient frequency in the soma and processes. Statistics were calculated by repeated measures one-way ANOVA followed by Tukey's multiple comparisons test, baseline and wash were not significantly different. Analysis window of  $\text{Ca}^{2+}$  free (4–13 min), wash (4–13 min) following exposure to solution.  $N$  (mice) = 3;  $n$  (cells) = 6. **f**, **g** 10 nM ET-1 (**f**), or 100 nM U46619 (**g**) increases  $\text{Ca}^{2+}$  transient frequency after 10 min exposure to  $\text{Ca}^{2+}$  free ACSF. Statistics were calculated by repeated measures one-way ANOVA followed by Šidák's multiple comparisons test.  $N$  = 2;  $n$  = 5 and  $N$  = 4;  $n$  = 7, respectively. For statistical comparisons \* $p$  < 0.05, \*\* $p$  < 0.01, \*\*\* $p$  < 0.001. All image scale bars, 10  $\mu\text{m}$ .

pericytes was robustly elevated by increasing extracellular  $\text{K}^{+}$  concentration from 2.5 mM to 60 mM and was significantly reduced in the presence of VGCC blockers (Fig. 2c–g and Tables S1 and S2, 1st to 3rd branch order from penetrating arteriole). In contrast, depolarization with 60 mM  $[\text{K}^{+}]_{\text{ex}}$  did not increase mid-capillary pericyte  $\text{Ca}^{2+}$  transient frequency (Fig. 2d) and VGCC blockers still had no effect on mid-capillary pericyte  $\text{Ca}^{2+}$  transient frequency when applied in 60 mM  $[\text{K}^{+}]_{\text{ex}}$  (Fig. 2c–g and Tables S1 and S2). To further test the effect of membrane voltage on mid-capillary pericyte  $\text{Ca}^{2+}$ , we pharmacologically altered  $\text{K}_{\text{ATP}}$  channel activity, whose modulation has been shown to have large effects on pericyte membrane

potential<sup>37–39</sup>. Consistent with our above results showing that mid-capillary  $\text{Ca}^{2+}$  transients were independent of VGCCs, application of pinacidil (10  $\mu\text{M}$ ), a  $\text{K}_{\text{ATP}}$  channel opener which hyperpolarizes pericytes, had no effect on transient frequency in processes or the soma (Fig. 2h). Furthermore, glibenclamide (20  $\mu\text{M}$ ) a  $\text{K}_{\text{ATP}}$  channel blocker, decreased rather than increased transient frequency in mid-capillary pericyte processes (Fig. 2i), suggesting that mid-capillary  $\text{K}_{\text{ATP}}$  channels were open at rest, and that depolarization may actually decrease  $\text{Ca}^{2+}$  influx. As a note, all experiments were performed in tetrodotoxin (TTX, 500 nM) to block neuronal action potentials, which alone had no significant effect on the frequency of mid-capillary pericyte  $\text{Ca}^{2+}$

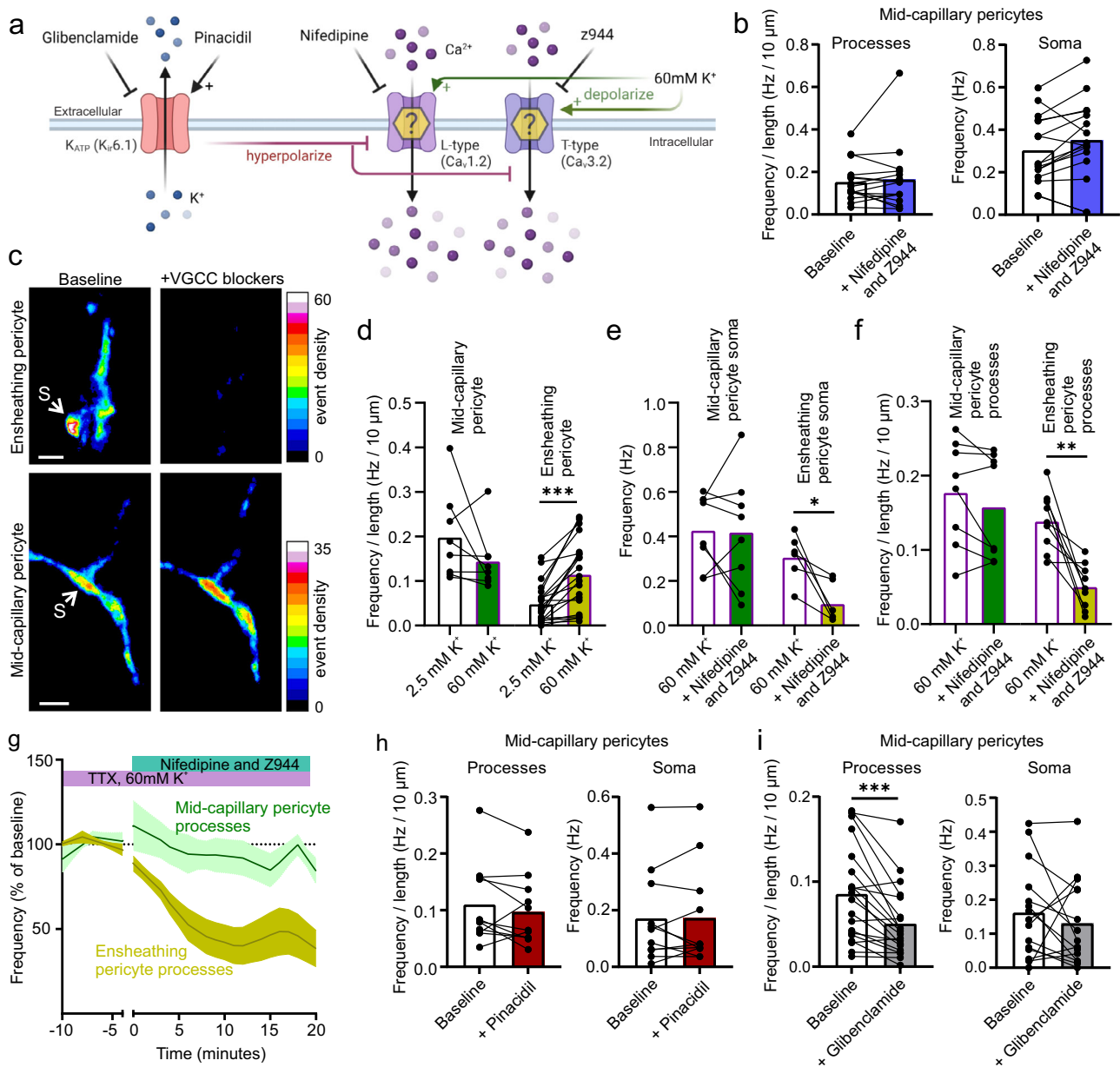


**Fig. 2** Mid-capillary pericyte  $\text{Ca}^{2+}$  transients are not potentiated by depolarization or mediated by VGCCs. **a** Schematic of experimental plan in Fig. 2. Created with biorender.com. **b** Blocking L-type and T-type VGCCs with  $20\ \mu\text{M}$  nifedipine and  $2\ \mu\text{M}$  Z944 does not reduce the frequency of  $\text{Ca}^{2+}$  transients in mid-capillary pericyte processes ( $N = 2, n = 16$ ) or soma ( $N = 2, n = 16$ ). Analysis was conducted 10–20 min after drugs reached the bath. **c** Example images showing event density (percentage of frames an event was detected within each pixel) after application of  $20\ \mu\text{M}$  nifedipine and  $2\ \mu\text{M}$  Z944 in  $60\ \text{mM}\ [\text{K}^+]_{\text{ex}}$  for an ensheathing pericyte (3rd order, top), and a mid-capillary pericyte (bottom). S points to soma. **d** Summarized data showing that changing  $[\text{K}^+]_{\text{ex}}$  from 2.5 to 60 mM does not increase the frequency of  $\text{Ca}^{2+}$  transients in mid-capillary pericytes (left,  $N = 2, n = 8$ ), but does significantly increase  $\text{Ca}^{2+}$  transient frequency of ensheathing pericytes (1st–3rd order,  $N = 2, n = 21$ ). Analysis done 9–18 min following  $60\ \text{mM}\ [\text{K}^+]_{\text{ex}}$  exposure. **e** Summarized data, showing application of  $20\ \mu\text{M}$  nifedipine and  $2\ \mu\text{M}$  Z944 in  $60\ \text{mM}\ [\text{K}^+]_{\text{ex}}$  reduces  $\text{Ca}^{2+}$  transient frequency in ensheathing ( $N = 5, n = 6$ ) but not mid-capillary pericyte soma ( $N = 4, n = 8$ ). Analysis was conducted 10–20 min after drugs reached the bath. **f** Summarized data, showing application of  $20\ \mu\text{M}$  nifedipine and  $2\ \mu\text{M}$  Z944 in  $60\ \text{mM}\ [\text{K}^+]_{\text{ex}}$  reduces  $\text{Ca}^{2+}$  transient frequency in ensheathing ( $N = 5, n = 9$ ) but not mid-capillary pericyte processes ( $N = 4, n = 8$ ). Analysis was conducted 10–20 min after drugs reached the bath. **g** Time course of data shown in **f**. **h** Summarized data of  $\text{K}_{\text{ATP}}$  channel opener  $10\ \mu\text{M}$  pinacidil on mid-capillary pericyte  $\text{Ca}^{2+}$  transient frequency in processes ( $N = 2, n = 11$ ), and soma ( $N = 2, n = 11$ ). Analysis was conducted 10–20 min after drugs reached the bath. **i** Summarized data of  $\text{K}_{\text{ATP}}$  channel blocker  $20\ \mu\text{M}$  glibenclamide on mid-capillary pericyte  $\text{Ca}^{2+}$  transient frequency in processes ( $N = 3, n = 20$ ), and soma ( $N = 3, n = 15$ ). Analysis was conducted 10–20 min after drugs reached the bath. All experiments performed in  $500\ \text{nM}$  TTX. Shaded area (**g**) represents SEM. Time 0 represents the start of the first 50 s acquisition in the presence of the new bathing solution (when the drug(s) are estimated to have reached the slice chamber). For statistical comparisons  $*p < 0.05$ ,  $**p < 0.01$ ,  $***p < 0.001$ . All image scale bars,  $10\ \mu\text{m}$ .



transients, consistent with a previous report<sup>18</sup>, although resting  $[Ca^{2+}]_i$  was slightly increased in TTX (Figs. S3 and S4 and Tables S1 and S2). Taken together, these results indicate that in contrast to ensheathing pericytes which exhibit elevated  $Ca^{2+}$  transients upon depolarization via VGCCs, mid-capillary pericyte  $Ca^{2+}$  transients are largely independent of VGCCs.

Having established a marked difference in the mechanisms of  $Ca^{2+}$  signaling between pericyte subtypes, we next examined the unidentified calcium influx pathway(s) required for the generation of  $Ca^{2+}$  transients in mid-capillary pericytes (Fig. 3a). We first tested the non-specific ion channel blocker SKF-96365, which was previously reported to block mid-capillary pericyte  $Ca^{2+}$  transients<sup>18</sup>. Consistent with this previous report,  $Ca^{2+}$  transient frequency in the processes and somas of these pericytes was largely diminished in the presence of SKF-96365 (100  $\mu$ M) (Fig. 3b and Tables S1 and S2). As SKF-96365 is a potent TRPC channel blocker, and TRPC3/6 are non-selective cation channels highly expressed in pericytes<sup>7</sup>, we further examined the sensitivity of mid-capillary pericyte  $Ca^{2+}$  transients to the TRPC3 blocker, Pyr3 and the potent TRPC3/6 blocker GSK-2833503A. Mid-capillary pericyte  $Ca^{2+}$  transients were unaffected by TRPC3 inhibition with Pyr3 (20  $\mu$ M), and inhibition of TRPC3/6 with GSK-2833503A (10  $\mu$ M) (Fig. 3b and Tables S1 and S2), suggesting influx via another SKF-96365 sensitive pathway. Interestingly, mid-capillary pericytes highly express Orai1 and Orai3  $Ca^{2+}$  channels<sup>7</sup>, and these channels are also sensitive to SKF-96365<sup>32</sup>. We therefore tested the sensitivity of mid-capillary pericyte  $Ca^{2+}$  transients to the non-selective Orai channel blocker 2-APB. 2-APB is a potent Orai1 channel blocker at high concentration but potentiates Orai1 channels at low concentrations<sup>40</sup>. Consistent with the bidirectional concentration-dependent sensitivity of Orai1 channels to 2-APB, 10  $\mu$ M 2-APB increased mid-capillary pericyte  $Ca^{2+}$  transient frequency, whereas 100  $\mu$ M 2-APB nearly abolished all transients (Fig. 3c and Tables S1 and S2). Although the effects of 2-APB are supportive of Orai mediated  $Ca^{2+}$  entry, 2-APB has several off-target effects, such as inhibiting  $IP_3$ Rs and some TRP channels. Therefore, we tested the sensitivity of mid-capillary pericyte  $Ca^{2+}$  transients to the Orai-specific blocker GSK-7975A<sup>41</sup>. Indeed, GSK-7975A (40  $\mu$ M) robustly reduced the frequency of  $Ca^{2+}$  transients in mid-capillary pericytes in both the soma and processes (Fig. 3d–g and Tables S1 and S2). Additionally, we tested the effects of the recently developed compound IA65, which enhances Orai1/3 but inhibits Orai2<sup>42,43</sup>. Consistent with the high mRNA expression of Orai1 and Orai3 in mid-capillary pericytes, IA65 (10  $\mu$ M) rapidly induced an elevation in resting  $Ca^{2+}$  levels (Fig. 3h and S4), although in contrast to 2-APB (10  $\mu$ M), we did not observe an increase in  $Ca^{2+}$  transient frequency (Tables S1 and S2).

While our data suggests that  $Ca^{2+}$  influx through Orai SOCE channels is required for the generation of spontaneous  $Ca^{2+}$  transients in mid-capillary pericytes, store-operated entry and store-release mechanisms are inextricably linked. Therefore, we set out to test the dependence of mid-capillary pericyte  $Ca^{2+}$  transients on store  $Ca^{2+}$  filling and release pathways (Fig. 4a). If mid-capillary pericyte  $Ca^{2+}$  transients were dependent on store release, then blocking store filling would be expected to block the generation of the transients. Indeed, pharmacological inhibition of the sarco(endo)-plasmic reticulum calcium-ATPase (SERCA), with cyclopiazonic acid (CPA, 30  $\mu$ M) abolished  $Ca^{2+}$  transients (Fig. 4b) suggesting their dependence on store release. In parallel to the drop in transient frequency, CPA induced a global and sustained resting  $Ca^{2+}$  elevation (Fig. 4b), consistent with the activation of Orai channels via ER  $Ca^{2+}$  depletion and STIM1/2 proteins. Given the dependence of the  $Ca^{2+}$  transients on store  $Ca^{2+}$ , we proceeded to investigate their dependence on the ER store release channels,  $IP_3$ Rs and RyRs. To test the relative

contributions of these channels to mid-capillary pericyte  $Ca^{2+}$  transients, we either inhibited phospholipase C with U73122 (which prevents  $IP_3$  production) or RyRs with the reversible antagonist tetracaine. Blocking  $IP_3$  production with U73122 (25  $\mu$ M) led a modest reduction in  $Ca^{2+}$  transient frequency in mid-capillary pericyte processes but not soma (Fig. 4c, d), and the spatial area of the remaining transients was also reduced (Fig. 4e). Strikingly, blocking RyRs with tetracaine (200  $\mu$ M) robustly reduced the frequency, spatial area, and duration of  $Ca^{2+}$  transients in mid-capillary pericyte processes and soma (Fig. 4g–j and Tables S1 and S2), as well as resting  $Ca^{2+}$  levels (Fig. S4). We additionally confirmed the reversibility of the tetracaine effect on transient frequency in five cells (200–500  $\mu$ M tetracaine =  $30.33\% \pm 8.610\%$ , washout =  $108.2\% \pm 25.01\%$  (% baseline frequency, mean  $\pm$  SEM);  $p = 0.0305$ , two-tailed paired Students' *t* test). Consistent with a functional role of RyRs in mid-capillary pericytes, application of caffeine (10 mM), a RyR potentiator, elevated mid-capillary pericyte  $Ca^{2+}$  (Fig. 4f). Altogether, these results point to a mechanism whereby constitutive  $Ca^{2+}$  entry through SOCE channels is required to maintain spontaneous  $Ca^{2+}$  release through RyRs and  $IP_3$ Rs, which in turn lead to store depletion and activation of Orai channels.

To confirm that the  $Ca^{2+}$  influx through Orai channels was indeed store-operated, we tested whether  $Ca^{2+}$  entry to maximal store depletion was also sensitive to Orai channel antagonists, by adapting a protocol commonly used to maximally activate SOCE in expression systems and cell culture<sup>44</sup>. First, we applied CPA (30  $\mu$ M) for 20 min in  $Ca^{2+}$ -free ACSF to deplete ER stores and maximally activate “store-operated” channels. Then, we reintroduced 1.2 mM  $[Ca^{2+}]_{ex}$  to the bathing solution while imaging a mid-capillary pericyte (Fig. 5a, b), triggering a large influx of  $Ca^{2+}$  through the open transmembrane channels. As expected, a large increase in mid-capillary pericyte  $Ca^{2+}$  was measured upon reintroduction of  $[Ca^{2+}]_{ex}$ , indicative of functional store-operated  $Ca^{2+}$  channels (Fig. 5a–c). As with the  $Ca^{2+}$  transients, this store depletion-induced  $Ca^{2+}$  influx was also sensitive to the Orai channel blockers, 2-APB and GSK-7975A, in mid-capillary pericytes (Fig. 5a, c). However, this experiment alone does not prove that store  $Ca^{2+}$  levels dictate the opening of the plasma membrane Orai channels, as the increase in cytoplasmic  $Ca^{2+}$  upon reintroduction of  $[Ca^{2+}]_{ex}$  could simply be occurring through store independent channels that are constitutively open. Therefore, we performed an experiment in which the brain slice was exposed to  $Ca^{2+}$ -free solution for the same duration as in the CPA experiments outlined above, but in the presence of tetracaine and U73122 to block store release via RyRs and  $IP_3$ Rs. If plasma membrane  $Ca^{2+}$  influx is truly controlled by ER store  $Ca^{2+}$  levels in mid-capillary pericytes, then the increase in  $[Ca^{2+}]_i$  upon reintroduction of  $[Ca^{2+}]_{ex}$  should be smaller than when stores are depleted and SOCE is activated. Indeed, in slices perfused with 200  $\mu$ M tetracaine and 25  $\mu$ M U73122, re-introduction of  $[Ca^{2+}]_{ex}$  resulted in a minute increase in  $Ca^{2+}$  entry that was not significantly different than when stores were depleted in the presence of Orai inhibitors (Fig. 5a, c). These results confirm that plasma membrane  $Ca^{2+}$  influx in mid-capillary pericytes is driven by ER store depletion.

The above evidence supporting SOCE channels in mid-capillary pericytes raised the intriguing possibility that Orai channels may be required to amplify and sustain GPCR mediated  $Ca^{2+}$  elevations, following robust release of  $Ca^{2+}$  from internal stores, as has been reported in other cell types (e.g. ref. <sup>45</sup>). Therefore, we harnessed the potent vasoconstrictor ET-1, which has been previously shown to induce large elevations in mid-capillary pericyte  $Ca^{2+}$ <sup>18</sup>. Indeed, in 1.2 mM  $[Ca^{2+}]_{ex}$ , ET-1 triggered a robust and sustained, but highly variable,  $Ca^{2+}$  elevation in mid-capillary pericytes (Fig. 6a, b). In contrast to the previously described role of the  $Ca^{2+}$  activated chloride channel,

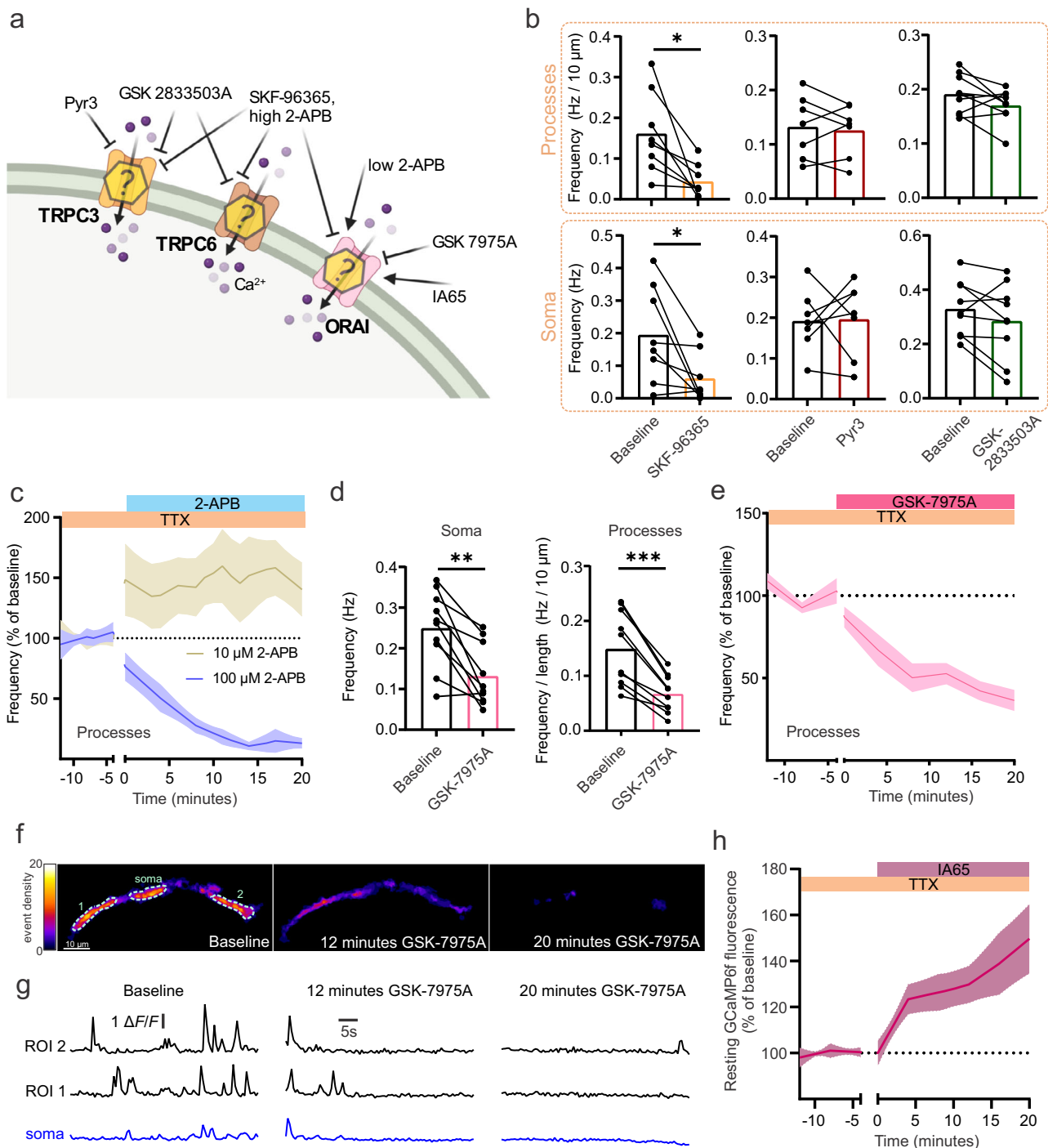


**Fig. 3** Mid-capillary pericyte  $\text{Ca}^{2+}$  transients signals are dependent on Orai  $\text{Ca}^{2+}$  channels. **a** Schematic of experimental plan and pharmacology. Created with biorender.com. **b** 100  $\mu\text{M}$  SKF-96365 reduces the frequency of  $\text{Ca}^{2+}$  transients in mid-capillary pericyte processes ( $N=3, n=8$ ) and soma ( $N=3, n=8$ ). Neither of the TRPC3 or the TRPC3/6 antagonists, 20  $\mu\text{M}$  Pyr3 or 10  $\mu\text{M}$  GSK-2833503A, significantly reduced pericyte  $\text{Ca}^{2+}$  transient frequency in soma ( $N=3, n=7$  and  $N=2, n=9$ , respectively) or processes ( $N=3, n=7$  and  $N=2, n=9$ , respectively). Analysis was conducted 10–20 min after drugs reached the bath. **c** Low concentration (10  $\mu\text{M}$ ) 2-APB increases whereas high concentration (100  $\mu\text{M}$ ) 2-APB reduces  $\text{Ca}^{2+}$  transient frequency in mid-capillary pericyte processes ( $N=3, n=9$  for both analyses). Analysis was conducted 10–20 min after drugs reached the bath. **d** The Orai channel inhibitor 40  $\mu\text{M}$  GSK-7975A reduces  $\text{Ca}^{2+}$  transient frequency in both soma (left,  $N=2, n=10$ ) and processes (right,  $N=2, n=10$ ). Analysis was conducted 10–20 min after drugs reached the bath. **e** Time course of data in (**d** right). **f** Event density image of a pericyte showing a decrease in  $\text{Ca}^{2+}$  transients at different time points following application of GSK-7975A. **g** Example traces of GCaMP6f signal over time in ROIs from soma and 2 regions of a pericyte's processes matching heat maps in **f**. **h** Perfusion of the Orai1/3 enhancer IA65 (10  $\mu\text{M}$ ) increases resting  $\text{Ca}^{2+}$  (GCaMP6f fluorescence measured in the soma,  $N=2, n=8$ ). All experiments performed in 500 nM TTX. Shaded areas represent SEM. Time 0 represents the start of the first acquisition in the presence of the new bathing solution (when the drug(s) are estimated to have reached the slice chamber). For statistical comparisons \* $p < 0.05$ , \*\* $p < 0.01$ , \*\*\* $p < 0.001$ .

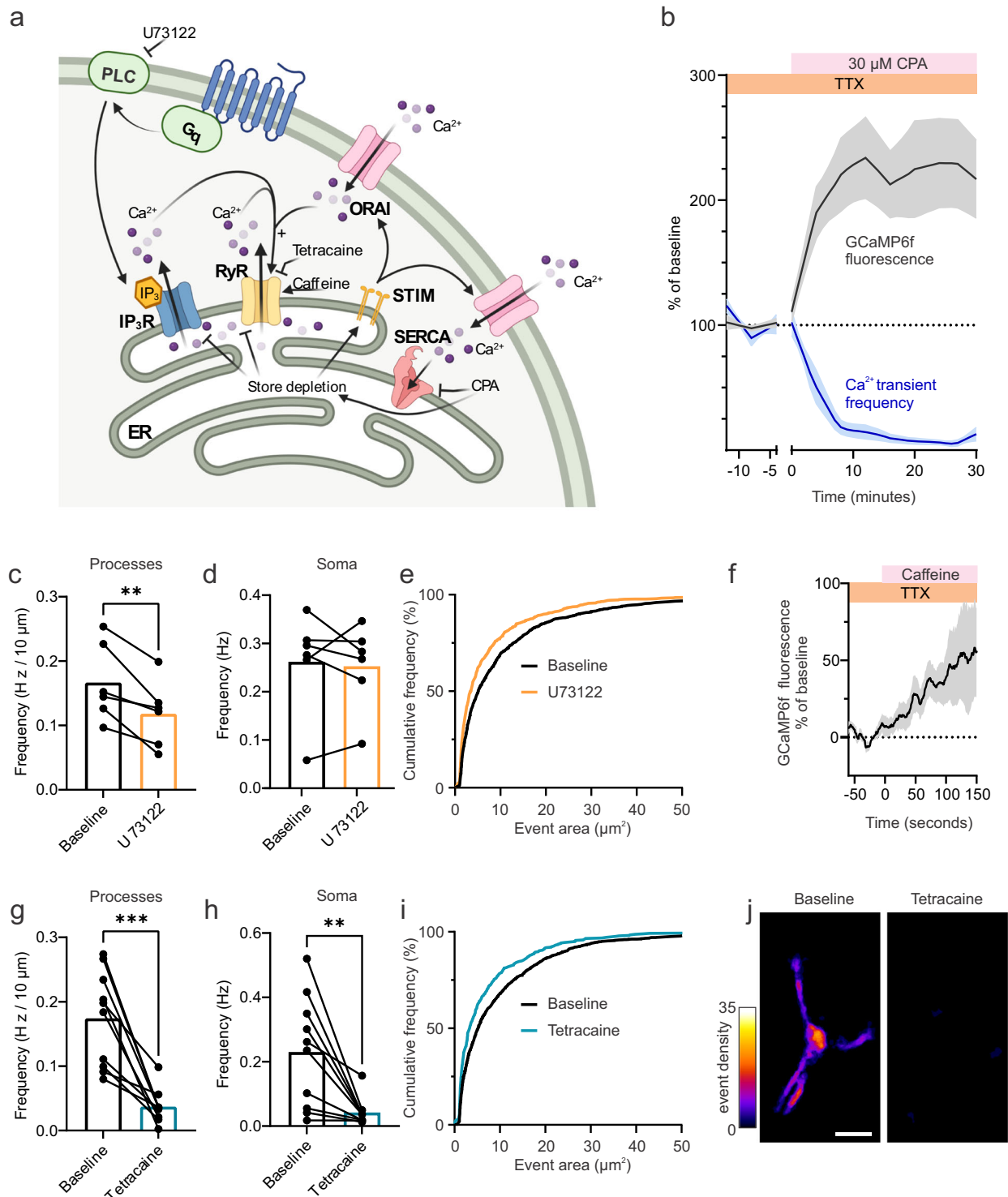


**Fig. 4** Mid-capillary pericyte  $\text{Ca}^{2+}$  transients are mediated by RyR and  $\text{IP}_3\text{R}$  store release pathways. **a** Schematic of experimental plan and pharmacology. Created with biorender.com. **b** Perfusion of cyclopiazonic acid (CPA 30  $\mu\text{M}$ ) to block SERCA pump and deplete intracellular stores, reduces the frequency of mid-capillary pericyte  $\text{Ca}^{2+}$  transients (blue trace), while elevating cytosolic  $\text{Ca}^{2+}$  (black trace).  $N = 4, n = 9$ . **c, d** Effect of phospholipase C inhibition with U 73122 (25  $\mu\text{M}$ ) on mid-capillary pericyte  $\text{Ca}^{2+}$  transient frequency measured in the processes (**c**,  $N = 2, n = 6$ ) and soma (**d**,  $N = 2, n = 6$ ). Analysis was conducted 10–20 min after drugs reached the bath. **e** Cumulative frequency plot showing reduction in event area in the presence of U 73122. **f** Caffeine (10 mM) increases cytosolic  $\text{Ca}^{2+}$  in mid-capillary pericytes (GCaMP6f fluorescence measured in the soma).  $N = 4, n = 9$ . **g, h** Effect of RyR inhibition with tetracaine (200  $\mu\text{M}$ ) on mid-capillary pericyte  $\text{Ca}^{2+}$  transient frequency measured in the processes (**g**,  $N = 3, n = 10$ ) and soma (**h**,  $N = 3, n = 10$ ). Analysis was conducted 10–20 min after drugs reached the bath. **i** Cumulative frequency plot showing reduction in event area in the presence of tetracaine (200  $\mu\text{M}$ ). **j** Heat map of event density in a mid-capillary pericyte before and after application of tetracaine (200  $\mu\text{M}$ ). Scale bar, 10  $\mu\text{m}$ . All experiments performed in 500 nM TTX. Shaded area (**b, f**) represents SEM. Time 0 represents the start of the first acquisition in the presence of the new bathing solution (when the solution is estimated to have reached the slice chamber). For statistical comparisons  $*p < 0.05$ ,  $**p < 0.01$ ,  $***p < 0.001$ .

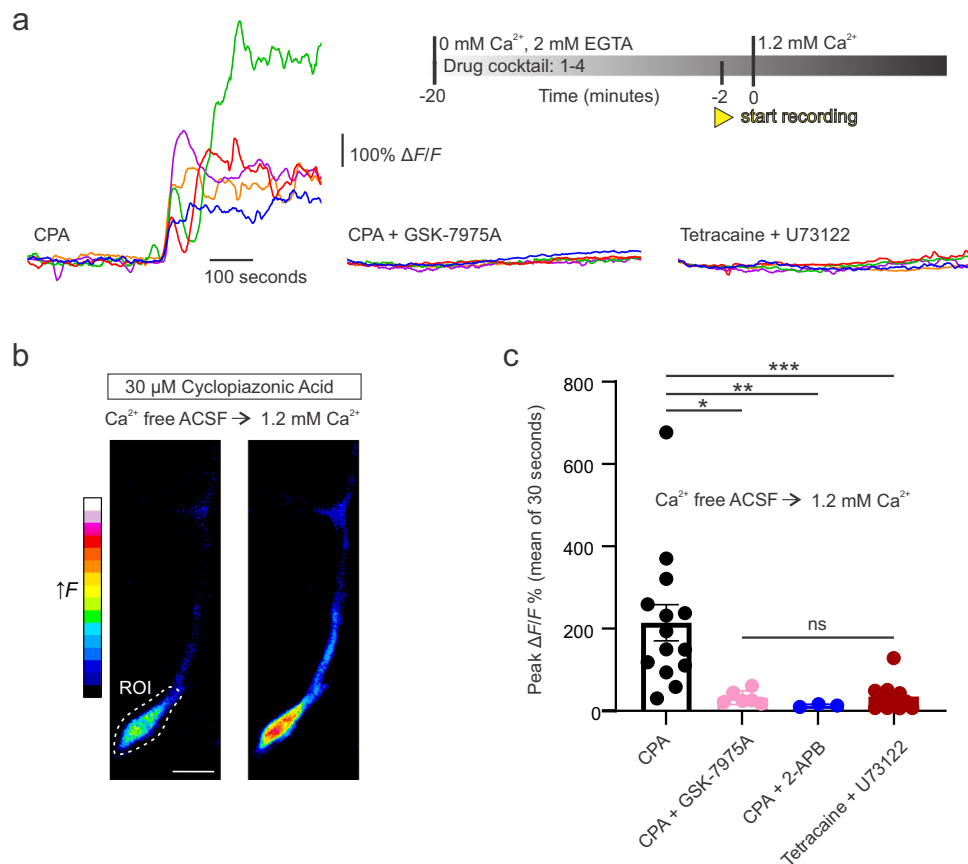


**Fig. 5** Mid-capillary pericytes express functional SOCE, that is blocked with Orai inhibitors. **a** Inset (top right), shows timing of experimental protocol. Five overlaid representative traces in different colors are shown in three different experimental conditions (left to right) from example cells in which 1.2 mM  $[Ca^{2+}]_{ex}$  is washed back on the brain slice. Left, in 30  $\mu$ M cyclopiazonic acid (CPA) to deplete ER stores and quantify the magnitude of  $Ca^{2+}$  entry via store-operated channels. Middle, same as left, but in the presence of the Orai inhibitor 40  $\mu$ M GSK-7975A. Right, wash back of  $Ca^{2+}$  in condition where store depletion is prevented by blocking RyR and  $IP_3R$  release pathways with tetracaine (200  $\mu$ M) and U73122 (25  $\mu$ M), respectively. **b** Example image showing increase in pericyte GCaMP6f fluorescence when extracellular ACSF is switched from  $Ca^{2+}$  free to 1.2 mM  $[Ca^{2+}]_{ex}$  in conditions where endoplasmic reticulum stores are depleted with 30  $\mu$ M CPA. An ROI around soma is used for quantification in **a** and **c**. Scale bar, 10  $\mu$ M. **c** Summarized data showing effect of ACSF ( $N = 8$ ,  $n = 14$ ), 40  $\mu$ M GSK-7975A ( $N = 2$ ,  $n = 6$ ), and 100  $\mu$ M 2-APB ( $N = 1$ ,  $n = 3$ ) on SOCE, following transition from 0 mM to 1.2 mM  $Ca^{2+}$  ACSF in the presence of 30  $\mu$ M CPA, and when store depletion is prevented by 200  $\mu$ M tetracaine and 25  $\mu$ M U 73122 ( $N = 2$ ,  $n = 11$ ). Statistics were calculated with a Kruskal-Wallis test followed by Dunn's multiple comparisons test. Error bars represent SEM. For statistical comparisons \* $p < 0.05$ , \*\* $p < 0.01$ , \*\*\* $p < 0.001$ .

TMEM16A, and VGCCs, which are required to amplify ET-1 mediated  $Ca^{2+}$  elevations in ensheathing type pericytes (1st–3rd branch orders)<sup>28</sup>, in mid-capillary pericytes, blocking VGCCs (20  $\mu$ M nifedipine and 2  $\mu$ M Z944) or TMEM16A (2  $\mu$ M Ani9) for 20 min had no significant effect on the magnitude of the ET-1 mediated  $Ca^{2+}$  elevation (Fig. 6a, b). However, when Orai channels were blocked with GSK-7975A for 20 min prior to ET-1 application, the magnitude of this elevation in  $[Ca^{2+}]_i$  was strongly reduced (Fig. 6a, b), and as in  $Ca^{2+}$ -free ACSF (Fig. S2), ET-1 evoked a transient increase in event frequency rather than a sustained elevation (Fig. 6c, d). Importantly, these  $Ca^{2+}$  elevations were prevented by U73122 (25  $\mu$ M, 20 min), confirming that ET-1 induced signals are initiated by the Gq-GPCR-PLC pathway (Fig. 6a, b). These results suggest that Orai mediated SOCE amplifies Gq-GPCR mediated  $Ca^{2+}$  elevations and may contribute to sustained increases in mid-capillary pericyte  $Ca^{2+}$  following the release of vasoconstrictive agents.

## Discussion

Here we demonstrate that spontaneous  $Ca^{2+}$  transients in mid-capillary brain pericytes are mediated by an interplay between

plasma membrane SOCE channels and ER store release through RyRs and  $IP_3Rs$ . Our results are suggestive of bidirectional coupling, whereby Orai transmembrane  $Ca^{2+}$  influx is required to sustain spontaneous  $Ca^{2+}$  release through RyRs and  $IP_3Rs$ , which in turn lead to store depletion and activation of Orai SOCE. These mechanisms are difficult to study in isolation: SOCE is dependent on store depletion, while store release is dependent on ER luminal  $Ca^{2+}$  load and intracellular  $Ca^{2+}$  levels, which are both heavily dictated by SOCE channels. Nevertheless, our pharmacological evidence, in conjunction with the short duration (~1–3 s) and spatially propagating nature of the observed  $Ca^{2+}$  transients, are consistent with a model in which spontaneous store release through RyRs and  $IP_3Rs$  is maintained by constitutive SOCE<sup>46,47</sup>. Orai channels are ideally suited due to their high  $Ca^{2+}$  selectivity and tight coupling with luminal  $[Ca^{2+}]$  in the ER via STIM proteins. Orai  $Ca^{2+}$  influx may additionally be critical for RyR activation by recruiting the intracellular  $Ca^{2+}$  required for calcium-induced-calcium-release (CICR) (e.g.,<sup>48</sup>), a mechanism which classically depends on L-type VGCCs in cardiac muscle<sup>49</sup> and in smooth muscle<sup>21</sup>.

Our study adds to a growing body of evidence that the mural cells of the cerebral vasculature represent a continuum, with



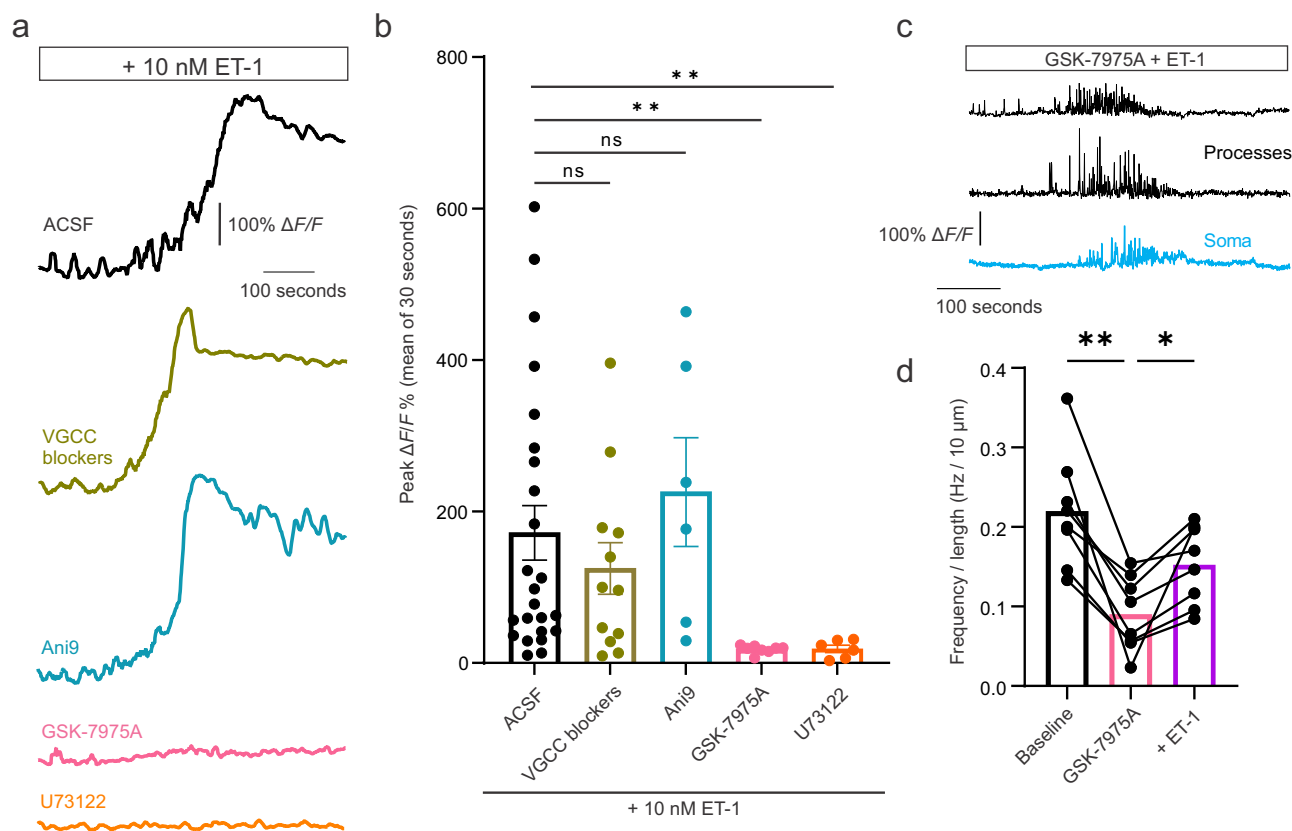


**Fig. 6**  $\text{Ca}^{2+}$  influx via Orai SOCE is required to sustain and amplify endothelin-1 induced  $[\text{Ca}^{2+}]_i$  elevations. **a**, **b** Example traces (**a**) and summarized data (**b**) in different experimental conditions showing ET-1 evokes large amplitude and sustained  $\text{Ca}^{2+}$  elevations when applied alone ( $N = 10$ ,  $n = 24$ ), and which is not dependent on VGCC channels (blocked with  $20 \mu\text{M}$  nifedipine +  $2 \mu\text{M}$  Z944;  $N = 3$ ,  $n = 12$ ) or the  $\text{Ca}^{2+}$  activated  $\text{Cl}^-$  channel, TMEM16A (blocked with  $2 \mu\text{M}$  Ani9;  $N = 3$ ,  $n = 6$ ). Blocking Orai  $\text{Ca}^{2+}$  channels with  $40 \mu\text{M}$  GSK-7975A reduces the ET-1 evoked rise in intracellular  $\text{Ca}^{2+}$  ( $N = 3$ ,  $n = 8$ ). Blocking phospholipase C with  $25 \mu\text{M}$  U73122 prevents ET-1 induced  $\text{Ca}^{2+}$  elevation ( $N = 2$ ,  $n = 6$ ), confirming it is dependent on GqGPCR-PLC pathway. Traces in **a** are temporally filtered with a 5 s running average. **c** Example trace showing that ET-1 induces a temporary increase in transient frequency when Orai channels are blocked with GSK-7975A (example is from the pericyte with the largest observed change in frequency). **d** Summarized data showing  $\text{Ca}^{2+}$  transient frequency increased (over a  $\sim 3$  min window), when ET-1 is added in the presence of GSK-7975A. Statistics were calculated with a Kruskal-Wallis test followed by Dunn's multiple comparisons test. All experiments performed in  $500 \text{ nM}$  TTX. Error bars represent SEM. For statistical comparisons  $*p < 0.05$ ,  $**p < 0.01$ ,  $***p < 0.001$ .

morphological, molecular, and functional heterogeneity along the arterio-venous axis. Our work is largely in agreement with a previous study which found that  $\text{Ca}^{2+}$  transients in mid-capillary pericyte processes were independent of L-type VGCCs at rest. However, in slight contrast to our results with  $20 \mu\text{M}$  nifedipine, a minimal decrease in  $\text{Ca}^{2+}$  transient frequency within the soma was reported with  $100 \mu\text{M}$  nimodipine<sup>18</sup>. Here we extend on these results and further show that these transients are not increased by depolarization and are likewise also independent of low-voltage-activated T-type calcium channels ( $\text{Ca}_v3.2$ ), which pericytes robustly express<sup>7</sup>. These findings contrast with our initial hypothesis that these transients would require VGCC activity, which was based on our previous finding that  $[\text{Ca}^{2+}]_i$  and  $\text{Ca}^{2+}$  transient frequency decreases in mid-capillary olfactory bulb pericytes following local increases in neuronal activity, although on a slower time scale than upstream ensheathing pericytes and SMCs<sup>9</sup>. While we show that VGCCs are not required for mid-capillary pericyte  $\text{Ca}^{2+}$  transients, they highly express both L- and T-type VGCCs<sup>7</sup> and it is possible that these channels become inactivated at  $\sim -20 \text{ mV}$  when exposed to  $60 \text{ mM}$   $[\text{K}^+]_{\text{ex}}$ . Therefore, we cannot conclude that these channels are entirely functionally absent, but rather that  $\text{Ca}^{2+}$  signaling in mid-capillary pericytes is dominated by other mechanisms, which we report here. Intriguingly, a concurrent study has reported that distal

retinal pericytes do show nifedipine-sensitive  $\text{Ca}^{2+}$  elevations in response to  $60 \text{ mM}$   $[\text{K}^+]_{\text{ex}}$ <sup>50</sup>. However, in contrast to SMCs and ensheathing pericytes, L-type VGCCs were not required for the  $\text{Ca}^{2+}$  elevation in retinal mid-capillary pericytes following increased intraluminal pressure<sup>50</sup>, consistent with our results exhibiting that  $\text{Ca}^{2+}$  transients in different subtypes of pericytes exhibit a differential dependence on VGCCs.

Our results in ensheathing pericytes are largely consistent with recent reports that have uncovered prominent roles of depolarization, L-type VGCCs, and Gq-GPCR-IP<sub>3</sub>R signaling in mediating their  $\text{Ca}^{2+}$  transients and  $[\text{Ca}^{2+}]_i$ <sup>27,28</sup>. Elucidating the molecular and functional differences between pericyte subtypes, including in the  $\text{Ca}^{2+}$  signaling mechanisms described here, remains an important task. While SOCE is universal across cell types, it is more prominent in non-excitable cells, perhaps due, in part, to the inhibition of VGCCs by the essential SOCE proteins STIM1 and STIM2<sup>51,52</sup>, raising the possibility that elevated STIM-plasma membrane interactions could have inhibitory effects on mid-capillary pericyte VGCCs. Another interesting possibility is differential inhibition by endogenous polyamines, such as spermine, which has been previously suggested to underlie the decreased functional expression of VGCCs in distal capillary pericytes of the retina<sup>30</sup>. How these signaling differences translate into functional differences remains another key point of future study.

Although our data suggests  $\text{Ca}^{2+}$  influx in mid-capillary pericytes occurs primarily via non-voltage-gated channels, this does not exclude a role for pericyte hyperpolarization in functional hyperemia. Several reports on pericyte membrane potential have been made in various preparations from different regions of the CNS, reporting mean resting membrane potentials of between  $-35$  mV and  $-50$  mV<sup>10,28,37–39,50</sup>. In pressurized intact retina preparations, pericytes across the vascular arbor are found more depolarized than smooth muscle cells at low pressure ( $-43$  mV vs.  $-64$  mV)<sup>50</sup>, suggesting pericytes have lower  $\text{K}^+$  permeability at rest. Opening of  $\text{K}_{\text{ATP}}$  channels increases  $\text{K}^+$  permeability of mid-capillary pericytes, and therefore causes a robust hyperpolarization<sup>37–39</sup>, which can then be propagated to upstream mural and endothelial cells<sup>37,39</sup>. Retrograde hyperpolarization is a robust phenomenon in the microvasculature which rapidly closes VGCCs on upstream SMCs and ensheathing pericytes, thereby decreasing intracellular  $\text{Ca}^{2+}$  and dilating these contractile cells to increase local cerebral blood flow<sup>9,27,53–55</sup>. Interestingly, we found that blocking  $\text{K}_{\text{ATP}}$  channels with glibenclamide led to a decrease in the frequency of  $\text{Ca}^{2+}$  transients, consistent with a decreased driving force for Orai mediated  $\text{Ca}^{2+}$  influx. This result suggests that  $\text{K}_{\text{ATP}}$  channels may be open at rest in pericytes from our brain slices, potentially due to increased adenosine tone which can open  $\text{K}_{\text{ATP}}$  channels via  $\text{A}_{2\text{A}}$  receptors<sup>37,38</sup>. Although modest increases in  $[\text{K}^+]_{\text{ex}}$  to 10 mM were previously suggested to decrease  $\text{Ca}^{2+}$  transient frequency via  $\text{K}_{\text{ATP}}$  dependent hyperpolarization<sup>18</sup>, unlike  $\text{K}_{\text{ir}2.x}$  channels,  $\text{K}_{\text{ATP}}$  channels are not known to be activated by  $[\text{K}^+]_{\text{ex}}$ . If  $\text{K}_{\text{ATP}}$  channels were indeed open at rest, as appears to be the case in our study, even modest increases in  $\text{K}^+$  would depolarize pericytes via these open  $\text{K}^+$  channels. Therefore, an alternative interpretation of these results could be that blocking  $\text{K}_{\text{ATP}}$  channels in their experiments blocked  $\text{K}^+$  induced depolarization rather than hyperpolarization, and thereby reduced driving force for  $\text{Ca}^{2+}$  entry via non-voltage-gated channels, consistent with our findings. Recordings of mid-capillary pericyte membrane potential changes in response to modest changes in  $\text{K}^+$  concentration are therefore needed to properly interpret these differences.

During neurovascular coupling, ensheathing pericytes of the capillary-arteriole transition zone (which robustly express  $\alpha$ -SMA) dilate rapidly, whereas the pericytes of the mid-capillary bed (low or negative for  $\alpha$ -SMA) increase their diameter more slowly<sup>9,56</sup>. Whereas ensheathing type pericytes dilate actively and independently from the arteriole<sup>10</sup>, it remains to be determined whether the mid-capillary diameter increase is a purely passive process or has an active component mediated by mid-capillary pericytes. Interestingly, under pathological conditions such as Alzheimer's disease and stroke, even mid-capillary pericytes are found to be constricted<sup>28,57</sup>, and prolonged optogenetic activation of ChR2 on cortical mid-capillary pericytes has been shown to locally constrict the capillaries that they contact on a slow timescale<sup>8,58</sup>. Likewise, increases in intraluminal pressure lead to mid-capillary pericyte depolarization in the retina, and are followed by a delayed constriction<sup>50</sup>. Although these studies suggest that mid-capillary pericyte membrane depolarization is correlated with increased rigidity and tone of the capillary bed, a causal relationship is lacking. Given that our data suggests that mid-capillary pericyte  $\text{Ca}^{2+}$  influx is dominated by voltage-independent channels, depolarization would be expected to reduce this  $\text{Ca}^{2+}$  influx and subsequent store filling, due to a decrease in driving force, as in other non-excitabile cells. This is consistent with a recent report showing that hyperpolarization of mid-capillary pericytes by application of pinacidil increased pressure-induced  $\text{Ca}^{2+}$  influx<sup>50</sup>.

Finally, we show here that SOCE is required to amplify the mid-capillary pericyte  $\text{Ca}^{2+}$  elevation mediated by the

vasoconstrictor ET-1. The magnitude of the ET-1-induced  $\text{Ca}^{2+}$  responses when applied in normal ACSF were highly variable, which could reflect heterogeneous expression of the endothelin-A receptor and/or SOCE proteins in mid-capillary pericytes. ET-1 is a central molecule to pericyte pathology, which is released in ischemia<sup>59</sup>, and which is elevated downstream of Amyloid- $\beta$  oligomers to constrict pericytes in Alzheimer's disease<sup>57</sup>. In ensheathing pericytes (1–3rd branch order), the ET-1 evoked  $[\text{Ca}^{2+}]_{\text{i}}$  increase was also recently shown to require an amplification step, but via  $\text{Ca}^{2+}$  activated  $\text{Cl}^-$  channel mediated depolarization and L-type VGCC activation<sup>28</sup>. Our results indicate a similar amplification process in mid-capillary pericytes, but with a clear molecular divergence in the mechanisms mediating ET-1 evoked  $\text{Ca}^{2+}$  influx. As  $\text{Ca}^{2+}$  is a ubiquitous signal transduction molecule throughout biology, mediating an array of cellular functions, including gene transcription and contraction, SOCE channels may therefore play an important role in numerous pericyte functions and contribute to their dysfunction in disease.

**Study limitations.** Genetic tools will ultimately be required to uncover the precise molecular identities underlying mid-capillary pericyte  $\text{Ca}^{2+}$  signaling. Our pharmacological modulation of SOCE with non-selective (SKF-96365 and 2-APB) and relatively selective (GSK-7975A and IA65) compounds is consistent with the highly  $\text{Ca}^{2+}$  selective family of Orai channels (namely, Orai1 and Orai3) as the molecular identities underlying pericyte SOCE. However, TRPC channels have been shown to interact with and contribute to SOCE in certain conditions<sup>60,61</sup>, although this concept is heavily debated<sup>62</sup>. While our results show that TRPC3/6 are not major contributors, we cannot completely rule out participation of the TRPC1/4/5 subfamily to pericyte SOCE.

The molecular identities of the  $\text{IP}_3\text{R}$  and RyR channels in mid-capillary pericytes will similarly require genetic tools to elucidate. While the  $\text{IP}_3\text{Rs}$  are broadly dispersed throughout cell types, the distribution of RyR isoforms is more segregated, with RyR2 constituting the dominant variant in smooth muscle cells<sup>63</sup>, making it the most likely variant to be functional in pericytes. Interestingly, RyRs have been classified as functionally absent in most<sup>64</sup> (but not all<sup>65,66</sup>) pericytes of different tissues, including ensheathing type pericytes in the retinal CNS vasculature<sup>27</sup>. It remains to be determined whether the functional expression of RyRs in cortical CNS mid-capillary pericytes represents a difference across brain regions and/or between pericyte subtypes.

Our study was conducted solely in the brain slice preparation, which is a highly useful tool for probing cellular signaling mechanisms, as pharmacological compounds can be delivered at a controlled concentration and cellular architecture is kept largely intact. However, there are important limitations when compared to in vivo settings: there is no blood pressure and myogenic tone, arterioles and capillaries are collapsed, oxygen concentration (95%) is supraphysiological, and the slice surface has undergone mechanical damage. Translation of this work to in vivo experimentation is an important future direction.

## Methods

**Ethics statement and animals.** All procedures conformed to the guidelines of the Canadian Council on Animal Care and were approved by the "Comité de déontologie sur l'expérimentation animale" (CDEA) of the Université de Montréal (QC, Canada). PDGFR $\beta$ -Cre mice<sup>67</sup> were crossed with Ai95(RCL-GCaMP6f)-D reporter mice (Jackson Laboratory) to obtain PDGFR $\beta$ -Cre; GCaMP6f-floxed double transgenic mice. Male and female mice aged P28–P163 were used in experiments.

**Acute brain slice preparation.** Prior to slicing, mice were put into deep anesthesia with isoflurane and 50  $\mu\text{L}$  of Rhodamine B isothiocyanate-Dextran (70 kDa, 2.5% wt:vol, Sigma-Aldrich) was injected retro-orbitally to label the vessel lumen. Mice were euthanized by decapitation. Following extraction from the skull, brains were placed into ice-cold NMDG-based slicing solution containing (in mM):

120 N-Methyl-D-glucamine, 3 KCl, 25 NaHCO<sub>3</sub>, 7 MgCl<sub>2</sub>·6H<sub>2</sub>O, 1 NaH<sub>2</sub>PO<sub>4</sub>·H<sub>2</sub>O, 20 Glucose, 2.4 Na-pyruvate, 1.3 Na-ascorbate, 1 CaCl<sub>2</sub>·H<sub>2</sub>O. Then, 300 μm thick coronal cortical slices were cut with a Leica VT 1200S Vibratome. Slices were transferred to a custom chamber with artificial cerebral spinal fluid (ACSF) containing (in mM): 126 NaCl, 2.5 KCl, 26 NaHCO<sub>3</sub>, 1.5 MgCl<sub>2</sub>·6H<sub>2</sub>O, 1.3 NaH<sub>2</sub>PO<sub>4</sub>·H<sub>2</sub>O, 10 Glucose, and 1.2 CaCl<sub>2</sub> at 36 °C for 10 min. Slices were then recovered in the chamber at room temperature until use. The fluorescent dye TO-PRO-3 has previously been shown to robustly label mid-capillary pericytes in fixed tissue<sup>34</sup>, and we have adapted this for imaging in acutely prepared live brain slices. Prior to use, slices were incubated in 1 μM TO-PRO-3 diluted in ACSF for 20 min at room temperature to label and identify the pericyte soma. All solutions used were continuously gassed with 95% O<sub>2</sub> and 5% CO<sub>2</sub>.

**Pharmacology and ion substitution.** All salts were obtained from Sigma-Aldrich. Please refer to Table S3 for identifiers, and vehicles of reagents used. Time 0 represents the start of the first acquisition when the new solution is estimated to have reached the bath (estimated based on the flow rate). For Ca<sup>2+</sup>-free ACSF, CaCl<sub>2</sub> was omitted from the ACSF and 2 mM EGTA was added. For 60 mM K<sup>+</sup> ACSF, equimolar NaCl was replaced with KCl. Slices were perfused with TTX for 10–20 min prior to imaging. For 60 mM K<sup>+</sup> experiments, slices were perfused with 60 mM K<sup>+</sup> for 10–20 min prior to application of VGCC blockers.

**Confocal imaging.** Imaging was performed with a Zeiss LSM 510 laser scanning confocal microscope with a 40X water immersion objective lens (0.8NA). Pericytes in cortical brain slices were located by TO-PRO-3 and GCaMP6f colocalization and association with a Rhodamine B labeled vessel. GCaMP6f was excited with a 488 nm LED laser and was detected after passing through a 505–530 nm bandpass filter. TO-PRO-3 and Rhodamine B were excited with a 633 nm and 543 nm HeNe laser respectively, which were generally turned off during Ca<sup>2+</sup> imaging. Ensheathing pericytes in a subset of explicitly labeled experiments were identified based on GCaMP fluorescence almost fully enveloping the vessel and were definitively confirmed to be within 3 branch orders of the penetrating arteriole. Mid-capillary pericytes were selected for all other experiments on the basis of: (1) Morphology: thin-stand or mesh morphology in which processes clearly did not fully envelop the vessel (notably different than those found on first 3 branches), (2) being positive for TO-PRO-3 labeling, and 3) the lack of an arteriole detected within 4 branches of the capillary using the Rhodamine B signal. In several cases for mid-capillary pericytes they could not be traced back 4 branches and an arteriole was not visible in the field of view, in these cases only criteria 1 and 2 were used. To measure calcium transient frequency over time, 50 s image acquisitions were made every 3–4 min in frame scanning mode at a 2 Hz sample rate. To record SOCE experiments and [Ca<sup>2+</sup>]<sub>i</sub> rises evoked by agonists, a single acquisition was made in frame scanning mode at a 2 Hz sample rate. Slices were perfused with ACSF at 2 mL/min and were kept at 34 ± 2 °C during experiments.

**Data collection and analysis.** Between frame XY-plane translational movement and within frame distortion were removed using a custom non-rigid alignment MATLAB algorithm, based on the *imregdemons* (AccumulatedFieldSmoothing = 2.5; PyramidLevels = 4; 32, 16, 8, and 4 iterations respectively for each pyramid level) and *imwarp* MATLAB functions (<https://scanbox.org/2016/06/30/non-rigid-image-alignment-in-twenty-lines-of-matlab/>). Hand-drawn regions of interest (ROI) separated pericyte somas from processes. The Astrocyte Quantification and Analysis (AQuA) MATLAB tool<sup>35</sup> was used for unbiased event-based Ca<sup>2+</sup> transient analysis. A Gaussian filter was applied to the images ( $\sigma = 2$ ), minimum event size was set to (pixels): 5/pixel size (μm), and detected events occurring in the same frame separated by (in pixels) 1/pixel size (μm) were merged. Event threshold parameters were set to reliably detect the majority of pericyte Ca<sup>2+</sup> signaling events with minimal detection of false events outside the cell boundaries. Identical analysis parameters were used for all time series of a given cell and experiment. In experiments in which movies were collected at differing timepoints and average data was shown, a linear interpolation between data points was performed. Ca<sup>2+</sup> transients following agonist application (ET-1 or U46619) in Ca<sup>2+</sup> free solution (Fig. 1f, g) or GSK-7975A (Fig. 6c, d) were only momentarily increased after agonist application before stores became depleted and were therefore analyzed over a brief period during which the agonists visibly evoked an increase in transient signals: ET-1 in Ca<sup>2+</sup>-free (65.2 ± 16.31 s); U46619 (78.86 ± 12.53 s); ET-1 in GSK-7975A (149.1 ± 7.841 s). To compare ET-1 responses at 5, 10, and 30 min in Ca<sup>2+</sup>-free solution (Fig. S2), Ca<sup>2+</sup> transient frequency following ET-1 application was analyzed over a 5 s timeframe from when the agonist first evoked signals. To examine changes in ensheathing pericyte Ca<sup>2+</sup> transient frequency following application of 60 mM [K<sup>+</sup>]<sub>ext</sub> an arteriole was located and single 50 s acquisitions of pericytes 1–3 branch orders downstream of the arteriole were taken before and 9–18 min after 60 mM [K<sup>+</sup>]<sub>ext</sub> application. Ca<sup>2+</sup> transient data during all other treatments in Figs. 2–4 was measured from 10–20 min after drug application unless otherwise stated. Transient frequency was normalized to 10 μm of pericyte processes (referred to as 'length'). To measure SOCE and [Ca<sup>2+</sup>]<sub>i</sub> rises evoked by ET-1 in Figs. 5–6, background fluorescence was subtracted, a hand-drawn ROI was placed around the soma, and ΔF/F was averaged 30 s around the peak value recorded. Event density heat maps in figures represent the fraction of frames in which

an active event was present in each pixel. To measure resting Ca<sup>2+</sup> levels (Fig. S4 and Table S1 and S2), a hand-drawn ROI was placed around the soma and an average fluorescence value was calculated from pixels in which AQuA did not detect an event for a given frame. Only cells in which the soma was in focus were included for this analysis. Five cells were excluded due to improper alignment of translational movement between recordings, and six cells were excluded as outliers following identification with the ROUT test ( $Q = 10\%$ ).

**Statistics.** For all paired data with two groups a two-tailed paired Students' *t* test was conducted. For paired data with three groups, a one-way repeated measures ANOVA was conducted, which if significant, was followed by Tukey's or Sidak's post-hoc test (see Figure Legends). For all other statistical comparisons normality was first assessed with a Shapiro–Wilk normality test. If this test failed, statistics were calculated by a Kruskal–Wallis non-parametric test, followed by Dunn's multiple comparisons test.

**Software availability.** Software used in the study is open source.

**Reporting summary.** Further information on research design is available in the Nature Portfolio Reporting Summary linked to this article.

## Data availability

Source data is available with the manuscript as Supplementary Data 1.

Received: 30 September 2022; Accepted: 21 April 2023;

Published online: 06 May 2023

## References

- Hartmann, D. A., Coelho-Santos, V. & Shih, A. Y. Pericyte control of blood flow across microvascular zones in the central nervous system. *Annu. Rev. Physiol.* **84**, 331–354 (2022).
- Grubb, S., Lauritzen, M. & Aalkjær, C. Brain capillary pericytes and neurovascular coupling. *Comp. Biochem. Physiol. Part Mol. Integr. Physiol.* **254**, 110893 (2021).
- Armulik, A., Genové, G. & Betsholtz, C. Pericytes: developmental, physiological, and pathological perspectives, problems, and promises. *Dev. Cell* **21**, 193–215 (2011).
- Grant, R. I. et al. Organizational hierarchy and structural diversity of microvascular pericytes in adult mouse cortex. *J. Cereb. Blood Flow Metab.* **39**, 411–425 (2017).
- Ratelade, J. et al. Reducing hypermuscularization of the transitional segment between arterioles and capillaries protects against spontaneous intracerebral hemorrhage. *Circulation* **141**, 2078–2094 (2020).
- Yang, A. C. et al. A human brain vascular atlas reveals diverse mediators of Alzheimer's risk. *Nature* **603**, 885–892 (2022).
- Vanlandewijck, M. et al. A molecular atlas of cell types and zonation in the brain vasculature. *Nature* **554**, 475 (2018).
- Hartmann, D. A. et al. Brain capillary pericytes exert a substantial but slow influence on blood flow. *Nat. Neurosci.* **24**, 633–645 (2021).
- Rungta, R. L., Chaigneau, E., Osmanski, B.-F. & Charpak, S. Vascular compartmentalization of functional hyperemia from the synapse to the pia. *Neuron* **99**, 362–375.e4 (2018).
- Hall, C. N. et al. Capillary pericytes regulate cerebral blood flow in health and disease. *Nature* **508**, 55–60 (2014).
- Armulik, A. et al. Pericytes regulate the blood-brain barrier. *Nature* **468**, 557–561 (2010).
- Daneman, R., Zhou, L., Kebede, A. A. & Barres, B. A. Pericytes are required for blood–brain barrier integrity during embryogenesis. *Nature* **468**, 562–566 (2010).
- Bell, R. D. et al. Pericytes control key neurovascular functions and neuronal phenotype in the adult brain and during brain aging. *Neuron* **68**, 409–427 (2010).
- Rustenhoven, J., Jansson, D., Smyth, L. C. & Dragunow, M. Brain pericytes as mediators of neuroinflammation. *Trends Pharmacol. Sci.* **38**, 291–304 (2017).
- Gerhardt, H. & Betsholtz, C. Endothelial-pericyte interactions in angiogenesis. *Cell Tissue Res.* **314**, 15–23 (2003).
- Dias, D. O. et al. Pericyte-derived fibrotic scarring is conserved across diverse central nervous system lesions. *Nat. Commun.* **12**, 5501 (2021).
- Nakagomi, T. et al. Brain vascular pericytes following ischemia have multipotential stem cell activity to differentiate into neural and vascular lineage cells. *Stem Cells* **33**, 1962–1974 (2015).



18. Glück, C. et al. Distinct signatures of calcium activity in brain mural cells. *Elife* **10**, e70591 (2021).
19. Hill, R. A. et al. Regional blood flow in the normal and ischemic brain is controlled by arteriolar smooth muscle cell contractility and not by capillary pericytes. *Neuron* **87**, 95–110 (2015).
20. Moosmang, S. et al. Dominant role of smooth muscle L-type calcium channel Cav1.2 for blood pressure regulation. *EMBO J.* **22**, 6027–6034 (2003).
21. Collier, M. L., Ji, G., Wang, Y.-X. & Kotlikoff, M. I. Calcium-induced calcium release in smooth muscle. *J. Gen. Physiol.* **115**, 653–662 (2000).
22. Knot, H. J. & Nelson, M. T. Regulation of arterial diameter and wall [Ca<sup>2+</sup>] in cerebral arteries of rat by membrane potential and intravascular pressure. *J. Physiol.* **508**, 199–209 (1998).
23. Nelson, M. T. et al. Relaxation of arterial smooth muscle by calcium sparks. *Science* **270**, 633–637 (1995).
24. Dabertrand, F., Nelson, M. T. & Brayden, J. E. Acidosis dilates brain parenchymal arterioles by conversion of calcium waves to sparks to activate BK channels. *Circ. Res.* **110**, 285–294 (2012).
25. Lin, Q. et al. IP<sub>3</sub> receptors regulate vascular smooth muscle contractility and hypertension. *JCI Insight* **1**, e89402 (2016).
26. Hill-Eubanks, D. C., Werner, M. E., Heppner, T. J. & Nelson, M. T. Calcium signaling in smooth muscle. *CSH Perspect. Biol.* **3**, a004549 (2011).
27. Gonzales, A. L. et al. Contractile pericytes determine the direction of blood flow at capillary junctions. *Proc. Natl Acad. Sci. USA* **117**, 27022–27033 (2020).
28. Korte, N. et al. The Ca<sup>2+</sup>-gated channel TMEM16A amplifies capillary pericyte contraction and reduces cerebral blood flow after ischemia. *J. Clin. Invest.* **132**, e154118 (2022).
29. Alarcon-Martinez, L. et al. Interpericyte tunnelling nanotubes regulate neurovascular coupling. *Nature* **585**, 91–95 (2020).
30. Matsushita, K. et al. Diabetes-induced inhibition of voltage-dependent calcium channels in the retinal microvasculature: role of spermine. *Investig. Ophthalmol. Vis. Sci.* **51**, 5979 (2010).
31. Singh, A., Hildebrand, M., Garcia, E. & Snutch, T. The transient receptor potential channel antagonist SKF96365 is a potent blocker of low-voltage-activated T-type calcium channels. *Br. J. Pharmacol.* **160**, 1464–1475 (2010).
32. Várnai, P., Hunyady, L. & Balla, T. STIM and Orai: the long-awaited constituents of store-operated calcium entry. *Trends Pharmacol. Sci.* **30**, 118–128 (2009).
33. Hariharan, A. et al. The ion channel and GPCR toolkit of brain capillary pericytes. *Front. Cell. Neurosci.* **14**, 601324 (2020).
34. Mai-Morente, S. P., Marsset, V. M., Blanco, F., Isasi, E. E. & Abudara, V. A nuclear fluorescent dye identifies pericytes at the neurovascular unit. *Neurochem.* **157**, 1377–1391 (2021).
35. Wang, Y. et al. Accurate quantification of astrocyte and neurotransmitter fluorescence dynamics for single-cell and population-level physiology. *Nat. Neurosci.* **22**, 1936–1944 (2019).
36. Tringham, E. et al. T-type calcium channel blockers that attenuate thalamic burst firing and suppress absence seizures. *Sci. Transl. Med.* **4**, 121ra19 (2012).
37. Sancho, M. et al. Adenosine signaling activates ATP-sensitive K<sup>+</sup> channels in endothelial cells and pericytes in CNS capillaries. *Sci. Signal.* **15**, eab15405 (2022).
38. Li, Q. & Puro, D. G. Adenosine activates ATP-sensitive K(+) currents in pericytes of rat retinal microvessels: role of A1 and A2a receptors. *Brain Res.* **907**, 93–99 (2001).
39. Hariharan, A., Robertson, C. D., Garcia, D. C. G. & Longden, T. A. Brain capillary pericytes are metabolic sentinels that control blood flow through a KATP channel-dependent energy switch. *Cell Rep.* **41**, 111872 (2022).
40. Prakriya, M. & Lewis, R. S. Potentiation and inhibition of Ca<sup>2+</sup> release-activated Ca<sup>2+</sup> channels by 2-aminoethylidiphenyl borate (2-APB) occurs independently of IP<sub>3</sub> receptors. *J. Physiol.* **536**, 3–19 (2001).
41. Derler, I. et al. The action of selective CRAC channel blockers is affected by the Orai pore geometry. *Cell Calcium* **53**, 139–151 (2013).
42. Azimi, I. et al. A new selective pharmacological enhancer of the Orai1 Ca<sup>2+</sup> channel reveals roles for Orai1 in smooth and skeletal muscle functions. *ACS Pharmacol. Transl. Sci.* **3**, 135–147 (2020).
43. Zhang, X. et al. Distinct pharmacological profiles of ORAI1, ORAI2, and ORAI3 channels. *Cell Calcium* **91**, 102281 (2020).
44. Bird, G. S., DeHaven, W. I., Smyth, J. T. & Putney, J. W. Methods for studying store-operated calcium entry. *Methods* **46**, 204–212 (2008).
45. Jairaman, A. et al. TREM2 regulates purinergic receptor-mediated calcium signaling and motility in human iPSC-derived microglia. *Elife* **11**, e73021 (2022).
46. Dupont, G., Combettes, L., Bird, G. S. & Putney, J. W. Calcium oscillations. *CSH Perspect. Biol.* **3**, a004226 (2011).
47. Yoast, R. E. et al. The native ORAI channel trio underlies the diversity of Ca<sup>2+</sup> signaling events. *Nat. Commun.* **11**, 2444 (2020).
48. Thakur, P., Dadsetan, S. & Fomina, A. F. Bidirectional coupling between ryanodine receptors and Ca<sup>2+</sup> release-activated Ca<sup>2+</sup> (CRAC) channel machinery sustains store-operated Ca<sup>2+</sup> entry in human T lymphocytes. *J. Biol. Chem.* **287**, 37233–37244 (2012).
49. Näbauer, M., Callewaert, G., Cleemann, L. & Morad, M. Regulation of calcium release is gated by calcium current, not gating charge, in cardiac myocytes. *Science* **244**, 800–803 (1989).
50. Klug, N. R. et al. Intraluminal pressure elevates intracellular calcium and contracts CNS pericytes: role of voltage-dependent calcium channels. *Proc. Natl Acad. Sci. USA* **120**, e2216421120 (2023).
51. Park, C. Y., Shcheglovitov, A. & Dolmetsch, R. The CRAC channel activator STIM1 binds and inhibits L-type voltage-gated calcium channels. *Science* **330**, 101–105 (2010).
52. Wang, Y. et al. The calcium store sensor, STIM1, reciprocally controls orai and CaV1.2 channels. *Science* **330**, 105–109 (2010).
53. Longden, T. A. et al. Capillary K<sup>+</sup>-sensing initiates retrograde hyperpolarization to increase local cerebral blood flow. *Nat. Neurosci.* **20**, 717 (2017).
54. Iadecola, C., Yang, G., Ebner, T. J. & Chen, G. Local and propagated vascular responses evoked by focal synaptic activity in cerebellar cortex. *J. Neurophysiol.* **78**, 651–659 (1997).
55. Chen, B. R., Kozberg, M. G., Bouchard, M. B., Shaik, M. A. & Hillman, E. M. A critical role for the vascular endothelium in functional neurovascular coupling in the brain. *J. Am. Heart Assoc.* **3**, e000787 (2014).
56. Rungta, R. L. et al. Diversity of neurovascular coupling dynamics along vascular arbors in layer II/III somatosensory cortex. *Commun. Biol.* **4**, 855 (2021).
57. Nortley, R. et al. Amyloid  $\beta$  oligomers constrict human capillaries in Alzheimer's disease via signaling to pericytes. *Science* **365**, eaav9518 (2019).
58. Nelson, A. R. et al. Channelrhodopsin excitation contracts brain pericytes and reduces blood flow in the aging mouse brain in vivo. *Front. Aging Neurosci.* **12**, 108 (2020).
59. Lampl, Y. et al. Endothelin in cerebrospinal fluid and plasma of patients in the early stage of ischemic stroke. *Stroke J. Cereb. Circ.* **28**, 1951–1955 (1997).
60. Molnár, T. et al. Store-operated calcium entry in müller glia is controlled by synergistic activation of TRPC and orai channels. *J. Neurosci.* **36**, 3184–3198 (2016).
61. Ong, H. L., Souza, L. Bde & Ambudkar, I. S. Role of TRPC channels in store-operated calcium entry. *Adv. Exp. Med. Biol.* **898**, 87–109 (2016).
62. DeHaven, W. I. et al. TRPC channels function independently of STIM1 and Orai1. *J. Physiol.* **587**, 2275–2298 (2009).
63. Westcott, E. B., Goodwin, E. L., Segal, S. S. & Jackson, W. F. Function and expression of ryanodine receptors and inositol 1,4,5-trisphosphate receptors in smooth muscle cells of murine feed arteries and arterioles. *J. Physiol.* **590**, 1849–1869 (2012).
64. Burdyga, T. & Borysova, L. Pericyte biology - novel concepts. *Adv. Exp. Med. Biol.* **1109**, 95–109 (2018).
65. Zhang, Q. et al. Membrane current oscillations in descending vasa recta pericytes. *Am. J. Physiol. Renal Physiol.* **294**, F656–F666 (2008).
66. Hashitani, H., Mitsui, R., Masaki, S. & Helden, D. F. Pacemaker role of pericytes in generating synchronized spontaneous Ca<sup>2+</sup> transients in the myenteric microvasculature of the guinea-pig gastric antrum. *Cell Calcium* **58**, 442–456 (2015).
67. Cuttler, A. S. et al. Characterization of Pdgfrb-Cre transgenic mice reveals reduction of ROSA26 reporter activity in remodeling arteries. *Genesis* **49**, 673–680 (2011).

## Acknowledgements

This work was supported by an NSERC discovery grant (RGPIN-2020-05276) to R.L.R.; R.L.R. holds a Canada Research Chair in Neurovascular Interactions. B.P. was supported by an USRA award from NSERC and a CIHR MSc Canada Graduate Scholarship. J.C. was supported by an USRA award from NSERC. The authors would like to thank Dr. Richard Robitaille (Université de Montréal) for gifting equipment, Dr. Terry Snutch (University of British Columbia) for gifting Z944, Dr. Mohamed Trebak (University of Pittsburgh) for gifting IA65, Dr. Volkhard Lindner (Maine Medical Center) for PDGFR $\beta$ -cre mice, and Dr. Isabel Laplante and Pierrette Kwemo for colony and lab management.

## Author contributions

B.P., E.M., and R.L.R. designed the study. B.P. and J.C. performed experiments. B.P., J.C., and R.L.R. analyzed data and interpreted results. E.M. developed analysis procedures. B.P. and R.L.R. wrote the manuscript with feedback from E.M.; R.L.R. supervised the research. All authors agreed on the final version of the manuscript.

## Competing interests

The authors declare no competing interests.

**Additional information**

**Supplementary information** The online version contains supplementary material available at <https://doi.org/10.1038/s42003-023-04858-3>.

**Correspondence** and requests for materials should be addressed to Ravi L. Rungta.

**Peer review information** *Communications Biology* thanks Søren Grubb and the other, anonymous, reviewer(s) for their contribution to the peer review of this work. Primary Handling Editors: Christian Wozny & Karli Montague-Cardoso.

**Reprints and permission information** is available at <http://www.nature.com/reprints>

**Publisher's note** Springer Nature remains neutral with regard to jurisdictional claims in published maps and institutional affiliations.



**Open Access** This article is licensed under a Creative Commons Attribution 4.0 International License, which permits use, sharing, adaptation, distribution and reproduction in any medium or format, as long as you give appropriate credit to the original author(s) and the source, provide a link to the Creative Commons license, and indicate if changes were made. The images or other third party material in this article are included in the article's Creative Commons license, unless indicated otherwise in a credit line to the material. If material is not included in the article's Creative Commons license and your intended use is not permitted by statutory regulation or exceeds the permitted use, you will need to obtain permission directly from the copyright holder. To view a copy of this license, visit <http://creativecommons.org/licenses/by/4.0/>.

© The Author(s) 2023